

# Multidimensional dynamics involving a conical intersection: Wavepacket calculations using the MCTDH method

G. A. Worth<sup>†</sup>, H.-D. Meyer<sup>\*</sup>, and L. S. Cederbaum<sup>\*</sup>

<sup>\*</sup> Theoretical Chemistry, University of Heidelberg, INF 229,  
69120 Heidelberg, Germany

<sup>†</sup> Dept. of Chemistry, King's College London, The Strand, London,  
WC2R 2LS, U.K.

This article will appear in *Conical Intersections*,  
W. Domcke, D. R. Yarkony, and H. Köppel, Eds.,  
World Scientific Co., (Singapore, 2004), pp. 573–607.

June 1, 2004

## 1 Introduction

The time-evolution of a molecular system through a conical intersection is multidimensional in nature, i.e. its description cannot be reduced to a single reaction coordinate. In addition to this, such processes are inherently quantum mechanical due to the mixing of electronic states as the intersection is traversed, and a powerful quantum dynamics method is required to treat these, often large, systems accurately.

The most intuitive way of obtaining a numerically exact solution of the time-dependent Schrödinger equation is to use standard wavepacket propagation methods. These represent the evolving system wavefunction using basis set expansion techniques or grid representations [1–3]. Unfortunately, the standard methods are restricted by an exponential increase in the computational resources required with the number of degrees of freedom treated, usually no more than 4–6 nuclear modes can be included. Systems in which vibronic coupling plays a role are often much larger than this. To treat these systems using the standard methods it is then necessary to turn to reduced dimensionality models in which only a few degrees of freedom are explicitly included, and the remainder either ignored or included in a phenomenological manner.

An alternative is to use approximative methods and include all degrees of freedom. In this chapter we discuss and apply the multi-configuration time-dependent Hartree (MCTDH) method [4–6]. At the present time, this method is the only one that can treat reliably, with controllable accuracy, the multi-mode dynamics of polyatomic systems like the ones discussed below. By using a time-dependent basis set that adapts with the evolving wavepacket, the MCTDH algorithm extends wavepacket propagation to larger systems. Importantly, calculations converge on the numerically exact solution and so the error introduced by the approximative nature of the method can be controlled. Using MCTDH, conically intersecting systems with up to 24 degrees of freedom have been studied.

Importantly, the vibronic coupling model Hamiltonian described in detail in section 2 is of a form that allows the full efficiency of the method to be realized. This combination of model and propagation technique thus allows us to study completely and in detail the multidimensional molecular dynamics through a conical intersection.

As well as providing an overview of the MCTDH methods and the vibronic coupling Hamiltonian, results will be presented in this chapter that highlight the features of three photo-physical systems in which vibronic coupling plays a crucial role. Here it will become clear that in some cases many degrees of freedom are required for a faithful description of system dynamics through a conical intersection, and for these the MCTDH method is able to provide accurate information.

## 2 Vibronic coupling Hamiltonian

The existence of a conical intersection within or close to the Franck-Condon zone has very dramatic effects on the dynamics and hence on the spectra of polyatomic molecules. Usually the density of spectral lines becomes very high and only the envelope, rather than the individual line, is of interest. This allows one to concentrate on short-time dynamics. For a reliable treatment of the dynamics it is important to describe the vicinity of the Franck-Condon point accurately. However, as only short-time dynamics is required, the interaction potential away from the Franck-Condon point may be of lesser accuracy.

The adiabatic potential energy surfaces in the vicinity of a conical intersection usually exhibit a rather complicated form, i.e. they are strongly anharmonic and may show double or multiple minima. In contrast to the adiabatic surfaces, the diabatic ones often show an astonishingly simple structure and may – for the region of interest – be well approximated by simple harmonic potentials. Combined with the fact that the diabatic coupling is well behaved, non-singular, and of potential type, this makes the diabatic representation extremely attractive.

We are interested in the study of absorption or ionisation spectra of small polyatomic molecules. Before the absorption of a photon (or the collision with an electron) the molecule is assumed to be in its electronic and vibrational ground state (we ignore rotation). We use the dimensionless normal coordinates of the ground state throughout and write the ground state Hamiltonian in harmonic approximation as

$$H_{GS} = T_n + \sum_{i=1}^f \frac{\omega_i}{2} Q_i^2 \quad (1)$$

$$T_n = - \sum_{i=1}^f \frac{\omega_i}{2} \frac{\partial^2}{\partial Q_i^2} \quad (2)$$

where  $f$  denotes the number of degrees of freedom and  $\omega_i$  is the  $i$ -th normal mode frequency (we use  $\hbar = 1$ ). The ground state is assumed to be well separated from all other electronic states. After excitation, however, the electronic structure is described by a set of close lying, interacting states. The vibronic Hamiltonian for this set of states reads

$$H = T_n + \mathbf{W}(\mathbf{Q}). \quad (3)$$

Assuming – for sake of simplicity – that there are only two interacting excited states of relevance and developing the diabatic potential energy matrix  $\mathbf{W}$  in a power series around the equilibrium position of the ground state and keeping only terms up to second order, one arrives at

$$\begin{aligned}
H &= T_n \mathbf{1} + \sum_{i=1}^f \frac{\omega_i}{2} Q_i^2 \mathbf{1} + \begin{pmatrix} \epsilon_1 & 0 \\ 0 & \epsilon_2 \end{pmatrix} \\
&+ \sum_{i \in G_1} \begin{pmatrix} \kappa_i^{(1)} & 0 \\ 0 & \kappa_i^{(2)} \end{pmatrix} Q_i \\
&+ \sum_{(i,j) \in G_2} \begin{pmatrix} \gamma_{i,j}^{(1)} & 0 \\ 0 & \gamma_{i,j}^{(2)} \end{pmatrix} Q_i Q_j \\
&+ \sum_{i \in G_3} \begin{pmatrix} 0 & \lambda_i \\ \lambda_i & 0 \end{pmatrix} Q_i \\
&+ \sum_{(i,j) \in G_4} \begin{pmatrix} 0 & \mu_{i,j} \\ \mu_{i,j} & 0 \end{pmatrix} Q_i Q_j. \tag{4}
\end{aligned}$$

The first two terms reproduce the ground state Hamiltonian, but located on the diagonal of the electronic  $2 \times 2$  matrix. The two energies  $\epsilon_1$  and  $\epsilon_2$  are the vertical excitation energies. The next four sums describe the linear and the bilinear coupling terms.

Due to symmetry considerations the sums run only over restricted sets of modes.  $G_1$  is the set of totally symmetric modes :

$$G_1 : \Gamma_i \supset \Gamma_A, \tag{5}$$

where  $\Gamma_i$  is the irreducible representation of the normal-mode coordinate  $Q_i$  and  $\Gamma_A$  the totally symmetric representation. These modes provide the linear intra-state coupling. They are called *tuning modes* as they modulate the energy gap between the two states.

$G_2$  is the set of pairs of modes that supplies the bilinear and quadratic on-diagonal couplings:

$$G_2 : \Gamma_i \times \Gamma_j \supset \Gamma_A. \tag{6}$$

The parameters  $\gamma_{i,j}^{(s)}$  account for frequency shifts and for the so-called Duschinsky rotation [7].

$G_3$  is the set of modes which provide linear coupling between the two interacting states :

$$G_3 : \Gamma_i \times \Gamma_1 \times \Gamma_2 \supset \Gamma_A, \tag{7}$$

where  $\Gamma_1$  and  $\Gamma_2$  are the irreducible representations of the two electronic states considered. These modes account for the linear inter-state coupling. They are called *coupling modes* as they couple the two electronic states. Finally,  $G_4$  is the set of all pairs of off-diagonal coupling modes which bilinearly enter the Hamiltonian:

$$G_4 : \Gamma_i \times \Gamma_j \times \Gamma_1 \times \Gamma_2 \supset \Gamma_A. \tag{8}$$

When only linear coupling terms are included, i. e. when  $\gamma$  and  $\mu$  are set to zero, one arrives at the so-called linear vibronic coupling (LVC) model.

A high symmetry of the molecule does not only help to (sometimes dramatically) reduce the number of parameters, it also provides a solid basis for the vibronic coupling model Hamiltonian. When the two interacting electronic states are of different symmetry (as assumed here), the inter-state coupling must be an odd function of the coupling coordinate. Hence there can be no constant or quadratic terms, only linear or bilinear ones are allowed. The vibronic coupling Hamiltonian was first derived by Cederbaum et. al. [8,9] and is more fully described in a review article by Köppel et. al. [10] and in Chapter II.1 of this book.

Quantum chemistry supplies us with the adiabatic potential energy surfaces  $V_i$ , and – at considerably higher cost – with the non-adiabatic coupling elements. Fortunately, the latter are not needed when determining the parameters of the vibronic coupling Hamiltonian, the knowledge of the adiabatic potential energy surfaces alone is sufficient. The parameters of the vibronic coupling Hamiltonian are determined by comparing the adiabatic potential energy surfaces obtained by diagonalising the diabatic model potential with those obtained by quantum chemistry. The most simple and most direct way is to require that the lowest order derivatives agree at the Franck-Condon point,  $\mathbf{Q} = 0$ . This readily yields for the linear parameters:

$$\kappa_i^{(s)} = \left. \frac{\partial V_s}{\partial Q_i} \right|_{\mathbf{Q}=0}, \quad (9)$$

$$\lambda_i^2 = \left. \frac{1}{8} \frac{\partial^2}{\partial Q_i^2} [V_2(\mathbf{Q}) - V_1(\mathbf{Q})]^2 \right|_{\mathbf{Q}=0}. \quad (10)$$

The equations for the parameters of the bilinear and quadratic terms are more complicated. They are discussed e. g. in Ref. [11].

It has been found, that the determination of the parameters may become unstable when going beyond the linear model. Much more convenient is then to determine the parameters by a least-squares fit, i. e. to minimize the function [12]

$$\begin{aligned} L(\kappa, \lambda, \gamma, \mu) = & \\ & \sum_{n=1}^{M_1} w_n^{(1)} [V_1^{mod}(\epsilon_1, \epsilon_2, \kappa, \lambda, \gamma, \mu; \mathbf{Q}_n) - V_1(\mathbf{Q}_n)]^2 \\ & + \sum_{n=1}^{M_2} w_n^{(2)} [V_2^{mod}(\epsilon_1, \epsilon_2, \kappa, \lambda, \gamma, \mu; \mathbf{Q}_n) - V_2(\mathbf{Q}_n)]^2. \end{aligned} \quad (11)$$

Here  $\kappa, \lambda, \gamma, \mu$  stand for all the coupling constants and  $V_{1,2}^{mod}$  denote the adiabatic surfaces obtained by diagonalising the potential part of the vibronic coupling Hamiltonian, Eq. (4). There is some unavoidable arbitrariness in this approach, as the points  $\mathbf{Q}_n$  and their weights  $w_n^{(s)}$  have to be chosen. However, the least-squares approach is to be preferred when more than linear coupling terms are included.

Finally we remark that one may replace the low order polynomials by other functions, if those functions would better describe the particular molecule under discussion. For example, the inter-state coupling mode of molecules like ethylene, allene, or butatriene is the torsion of the two  $\text{CH}_2$  end-groups. To correctly reproduce the periodicity of this degree of freedom one may replace  $\lambda Q$  by  $\alpha \sin(\beta Q)$ , where  $\alpha\beta = \lambda$  and where  $Q$  is the normal mode coordinate representing the torsion [12].

## 3 Multiconfiguration Time-Dependent Hartree (MCTDH)

### 3.1 Introduction

Wavepacket propagation methods are an essential tool for understanding the molecular dynamics underlying many physical phenomena, especially those that occur on an ultrafast (sub-picosecond) time scale. The standard method is the numerically exact solution of the time-dependent Schrödinger equation, representing the wavepacket and Hamiltonian in an appropriate basis. The method is however restricted by the numerical resources required, which grow exponentially with the number of

degrees of freedom, and studies of systems with more than six degrees of freedom are in general impossible.

In an attempt to remove this obstacle, approximate methods exemplified by the time-dependent Hartree (TDH) method have been developed. Here, the wavefunction is represented as a Hartree product of one-dimensional functions, and as a result the equations of motion for the wavepacket are a set of coupled one-dimensional equations. The effort required is thus significantly reduced, but at the cost that the correlation between the degrees of freedom is no longer treated correctly. For strongly correlated systems like the vibronic coupled ones, TDH completely fails.

The multiconfiguration time-dependent Hartree (MCTDH) method [4–6, 13, 14] combines the benefits of these two extremes. As the name implies, the wavefunction is described by an expansion in Hartree products (configurations). Using this wavefunction ansatz and solving the time-dependent Schrödinger equation by a variational method leads to a set of coupled equations of motion for the expansion coefficients and for the functions used to build the Hartree products. The latter are known as *single-particle functions* (SPFs). In the limit of convergence with respect to the number of configurations included, the results become numerically exact. An important feature of the method is that, due to its variational character, small sets of SPFs are in general sufficient to produce good results. The MCTDH method thus requires considerably less effort and memory than the standard one.

### 3.2 Equations of Motion

The MCTDH method is to a large extent defined through its *ansatz* for the wavefunction [4–6, 13]

$$\Psi(Q_1, \dots, Q_f, t) = \sum_{j_1=1}^{n_1} \dots \sum_{j_f=1}^{n_f} A_{j_1 \dots j_f}(t) \prod_{\kappa=1}^f \varphi_{j_\kappa}^{(\kappa)}(Q_\kappa, t), \quad (12)$$

where  $f$  denotes the number of degrees of freedom,  $Q_1, \dots, Q_f$  are the nuclear coordinates, the  $A_{j_1 \dots j_f}$  denote the MCTDH expansion coefficients, and the  $\varphi_{j_\kappa}^{(\kappa)}$  are the  $n_\kappa$  expansion functions for each degree of freedom  $\kappa$ , the SPFs.

We simplify the notation by introducing the composite index  $J$

$$J = (j_1, j_2, \dots, j_f), \quad (13)$$

and the configuration

$$\Phi_J = \prod_{\kappa=1}^f \varphi_{j_\kappa}^{(\kappa)}, \quad (14)$$

which is known as a *Hartree product*. The MCTDH wavefunction is thus a superposition of Hartree products. This explains the name of the method. Alternatively one may interpret Eq. (12) as an expansion of the wavefunction in a time-dependent product basis. Since the basis set functions follow the wavepacket, one may expect that the numbers,  $n_\kappa$ , of SPFs, needed to ensure convergence, are rather small. The SPFs are given only numerically, and in a practical calculation they thus have to be represented in an underlying – so-called primitive – basis set

$$\varphi_{j_\kappa}^{(\kappa)}(q_\kappa, t) = \sum_{l=1}^{N_\kappa} c_{l j_\kappa}^{(\kappa)}(t) \chi_l^{(\kappa)}(q_\kappa).$$

MCTDH will be of advantage if  $n_\kappa < N_\kappa$  ( $\kappa = 1, \dots, f$ ). The primitive basis functions  $\chi_l^{(\kappa)}$  are in practice often replaced by a discrete variable representation (DVR) grid [6, 15, 16], and we use the word *grid* as synonymous with *primitive basis*.

The equations of motion for the coefficients and the SPFs are derived from the Dirac-Frenkel variational principle [17, 18]

$$\langle \delta\Psi | H - i\partial/\partial t | \Psi \rangle = 0. \quad (15)$$

As the coefficients and the SPFs are time-dependent, there are some ambiguities in the equations of motions which must be lifted by imposing constraints. The simplest set of constraints reads

$$\langle \varphi_j^{(\kappa)}(t) | \dot{\varphi}_l^{(\kappa)}(t) \rangle = 0. \quad (16)$$

These constraints minimise the motion of the SPFs and keeps them orthonormal. For a discussion of other constraints see Ref. [5, 6]. Employing the above constraints, the equations of motion read [5, 6]

$$i\dot{A}_J = \sum_L \langle \Phi_J | H | \Phi_L \rangle A_L, \quad (17)$$

$$i\dot{\varphi}_j^{(\kappa)} = \sum_{l,m} \left(1 - P^{(\kappa)}\right) \left(\rho^{(\kappa)-1}\right)_{jl} \langle \mathbf{H} \rangle_{lm}^{(\kappa)} \varphi_m^{(\kappa)} \quad (18)$$

where

$$P^{(\kappa)} = \sum_{j=1}^{n_\kappa} |\varphi_j^{(\kappa)}\rangle \langle \varphi_j^{(\kappa)}| \quad (19)$$

denotes the projector on the space spanned by the SPFs for the  $\kappa$ th degree of freedom, and

$$\rho_{jl}^{(\kappa)} = \langle \Psi_j^{(\kappa)} | \Psi_l^{(\kappa)} \rangle \quad (20)$$

and

$$\langle \mathbf{H} \rangle_{jl}^{(\kappa)} = \langle \Psi_j^{(\kappa)} | H | \Psi_l^{(\kappa)} \rangle \quad (21)$$

denote a *density matrix* and a matrix of *mean-fields*, respectively. Here

$$\Psi_l^{(\kappa)} = \langle \varphi_l^{(\kappa)} | \Psi \rangle_\kappa \quad (22)$$

denotes a *single-hole function*. Obviously,  $\Psi_l^{(\kappa)}$  depends on all coordinates except the  $\kappa$ 's one. The mean-fields are thus one-dimensional operators, acting solely on the  $\kappa$ 's degree of freedom.

The MCTDH equations of motion (17,18) are a fairly complicated set of coupled non-linear differential equations. (Note that  $\dot{A}$  depends on  $\varphi$  through  $\langle \Phi_J | H | \Phi_L \rangle$  and  $\dot{\varphi}$  depends on  $A$  through  $\rho$  and  $\langle \mathbf{H} \rangle$ ). However, there are fewer equations compared to the set of linear differential equations of the standard method, i.e by simply employing directly the primitive product basis set. In fact, the number of equations is often smaller by several orders of magnitude. This is what makes MCTDH both small and fast.

### 3.3 Representation of the Hamiltonian

The solution of the MCTDH equations of motion requires the evaluation of the Hamiltonian matrix  $\langle \Phi_J | H | \Phi_L \rangle$  and the mean fields  $\langle \mathbf{H} \rangle$  at each time step of the integration. These are formally  $f$  and  $f-1$  dimensional integrals. Doing the integrals by multi-dimensional quadrature over the primitive grid points would slow down MCTDH such that it would not be competitive.

The multi-dimensional integrations can be circumvented if the Hamiltonian is written as a sum of products of single-particle operators,

$$H = \sum_{r=1}^s c_r \prod_{\kappa=1}^f h_r^{(\kappa)}, \quad (23)$$

with expansion coefficients  $c_r$ . Using Eq. (23) the matrix elements can be expanded as

$$\langle \Phi_J | H | \Phi_L \rangle = \sum_{r=1}^s c_r \prod_{\kappa=1}^f \langle \varphi_{j_\kappa}^{(\kappa)} | h_r^{(\kappa)} | \varphi_{l_\kappa}^{(\kappa)} \rangle, \quad (24)$$

and similarly for the mean fields (see Ref. [5,6]). Note that only one-dimensional integrals are used now. Fortunately, the vibronic-coupling Hamiltonian, derived in the previous section, is precisely of form (23) with comparatively few expansion terms. This makes MCTDH very well adapted for solving the vibronic coupling dynamical problem.

For the general case we remark that the kinetic energy operator normally has the required form (23), but the potential energy operator often does not. It then may be fitted to the product form. A convenient, systematic, and efficient approach to obtain an optimal product representation is described in Refs. [6,19]. We finally note that there are other methods which evaluate the Hamiltonian matrix elements efficiently without relying on a product expansion (23). Most notable here is the CDVR method of Manthe [20].

The building of the mean fields is still the most time consuming part of MCTDH. To reduce the effort, the mean fields are evaluated not at every integrator time step but at larger (so called *update*) time steps. This *constant mean field* (CMF) integration scheme is described in Refs. [6,21]. The use of CMF speeds up the calculation by typically a factor of 10.

### 3.4 Non-adiabatic systems

It was implicitly assumed in the discussion so far, that the motion of the molecular nuclei is determined by a single Born-Oppenheimer potential energy surface. However, in vibronic coupling systems, there are several coupled electronic states of importance. The MCTDH algorithm hence has to be extended to deal with more than one electronic state.

The most direct way to accomplish this is to choose one extra degree of freedom, the  $\kappa_e$ th say, to represent the electronic manifold [22,23]. The coordinate  $Q_{\kappa_e}$  then labels the electronic states, taking only discrete values  $Q_{\kappa_e} = 1, 2, \dots, \sigma$ , where  $\sigma$  is the number of electronic states under consideration. The number of SPFs for such an electronic mode is set to the number of states, i.e.  $n_{\kappa_e} = \sigma$ . The equations of motion (17) and (18) remain unchanged, treating nuclear and electronic modes on the same footing. This is called the *single-set formulation*, since only one set of SPFs is used for all the electronic states.

Contrary to this, the *multi-set formulation* employs different sets of SPFs for each electronic state [24,25]. In this formulation the wavefunction  $\Psi$  and the Hamiltonian  $H$  are expanded in the set  $\{|\alpha\rangle\}$  of electronic states:

$$|\Psi\rangle = \sum_{\alpha=1}^{\sigma} \Psi^{(\alpha)} |\alpha\rangle \quad (25)$$

and

$$H = \sum_{\alpha,\beta=1}^{\sigma} |\alpha\rangle H^{(\alpha\beta)} \langle\beta|, \quad (26)$$

where each state function  $\Psi^{(\alpha)}$  is expanded in MCTDH form (12). The derivation of the equations of motion corresponds to the single-set formalism, except that extra state labels have to be introduced on the various quantities such as mean fields and

density matrices. The equations of motion now read

$$i\dot{A}_J^{(\alpha)} = \sum_{\beta=1}^{\sigma} \sum_L \langle \Phi_J^{(\alpha)} | H^{(\alpha\beta)} | \Phi_L^{(\beta)} \rangle A_L^{(\beta)}, \quad (27)$$

$$i\dot{\varphi}_j^{(\alpha,\kappa)} = \sum_{lm\beta} \left(1 - P^{(\alpha,\kappa)}\right) \left(\rho^{(\alpha,\kappa)}\right)^{-1}_{jl} \langle \mathbf{H} \rangle_{lm}^{(\alpha\beta,\kappa)} \varphi_m^{(\beta,\kappa)}, \quad (28)$$

with mean-fields

$$\langle H \rangle_{jl}^{(\alpha\beta,\kappa)} = \langle \Psi_j^{(\alpha,\kappa)} | H^{(\alpha\beta)} | \Psi_l^{(\beta,\kappa)} \rangle. \quad (29)$$

The superscripts  $\alpha$  and  $\beta$  denote to which electronic state the functions and operators belong. A fuller derivation of these equations is given in Ref. [6, 21, 25].

The single-set formulation is to be preferred when the different electronic states have a similar form. The well known spin-boson model is in this category [26]. When the motion on the different electronic states is very different, the multi-set formulation becomes the appropriate choice. The smaller number of SPFs needed for convergence then over-compensates the overhead of the multi-set formulation. For vibronically coupled systems, we have always chosen the multi-set formulation.

### 3.5 Mode combination

The importance of the memory requirements for large systems can be easily seen by looking at what would be needed for studying the dynamics of the pyrazine molecule ( $C_4H_4N_2$ ). This system has 25 degrees of freedom (24 vibrational modes and a set of electronic states). Although in a study we have performed [14] the mean grid length for the degrees of freedom was only  $N \approx 7.4$ , the corresponding direct product grid consists of about  $10^{21}$  points making the use of the standard method totally infeasible. Unfortunately, the MCTDH method as presented above, using a set of SPFs per degree of freedom, is also unable to treat this system on a workstation: the program requires memory equivalent to approximately 12 wavefunction vectors, double precision complex, and so with only 5 SPFs for each of the four strongly coupled modes and only 2 SPFs per mode for the remaining degrees of freedom the calculation would need  $5^4 \times 2^{21} \times 12 \times 16$  Bytes  $\approx 234$  GB.

The memory requirements can however be reduced if SPFs are used that describe a set of degrees of freedom, rather than just one. The wavefunction ansatz, Eq. (12), is then rewritten as a multi-configuration over  $p$  generalised ‘‘particles’’,

$$\Psi(q_1, \dots, q_p, t) = \sum_{j_1=1}^{\tilde{n}_1} \dots \sum_{j_p=1}^{\tilde{n}_p} A_{j_1 \dots j_p}(t) \prod_{\kappa=1}^p \varphi_{j_\kappa}^{(\kappa)}(q_\kappa, t), \quad (30)$$

where  $q_\kappa = (Q_i, Q_j, \dots)$  is the set of coordinates combined together in a single particle, described by  $\tilde{n}_\kappa$  functions, termed *multi-mode* SPFs to distinguish them from the usual *single-mode* SPFs.

By combining  $d$  degrees of freedom together to form a set of  $p = f/d$  particles, the memory requirement reads

$$\text{memory} \sim p\tilde{n}N^d + \tilde{n}^p, \quad (31)$$

where  $\tilde{n}$  is the number of multi-mode functions needed for the new particles. The first and second term of Eq. (31) represent the space taken by the SPFs and the coefficients, respectively. This equation holds as well for the uncombined case when setting  $p = f, d = 1$  and  $\tilde{n}_\kappa = n_\kappa$ . For large systems, the second term of Eq. (31) dominates. Thus if

$$\tilde{n} < n^d, \quad (32)$$

i.e. the number of multi-mode functions is less for a multi-dimensional particle than the product of single-mode functions needed for the separate degrees of freedom, there can be a large saving in memory required.

The inequality (32) will in general be fulfilled. This comes from the fact that the number of SPFs required is related to the strength of coupling between the particle and the rest of the system. By combining modes, this coupling is reduced as the coupling between the combined degrees of freedom is now treated within the SPFs for the combined mode. For example, consider a system with a set of coupled modes. The coupling will lead to a wavefunction which is poorly described by a Hartree product, and many single-mode SPFs would be needed. Going to the extreme and combining all the degrees of freedom together into one particle, only one SPF will be required: the standard numerically exact wavefunction.

To summarize, if only single-mode functions are used, i.e.  $d = 1$ , the memory requirement is dominated by the number of  $A$ -coefficients,  $n^f$ . By combining degrees of freedom together this number can be reduced, but at the expense of longer product grids required to describe the now multi-mode SPFs. At the extreme of all degrees of freedom combined together, one arrives at  $N^f$ . Between these two extremes however, there is an optimally small amount of memory required. Similar considerations apply to the numerical effort. For a fuller discussion see Ref. [6]. Combining modes is not recommended for small systems, unless two degrees of freedom are very strongly coupled [27]. For large systems however, the effect is very significant, and enables the 24 nuclear degrees of freedom pyrazine system to be studied [11, 14, 28]. More recently it was even possible to study a 80 mode spin-boson model with the MCTDH method [26] using highly combined SPFs.

## 4 Examples of dynamics

### 4.1 Spectral Intensities

In this section results are presented from MCTDH wavepacket propagation calculations [29] on systems involving a conical intersection. The accuracy of the method is such that all results can be taken as complete quantum dynamical calculations, while the power is seen in that calculations with up to 24 vibrational modes have been made, allowing calculations to be made without resorting to drastic approximations. Photophysical systems from three molecules will be looked at: butatriene, allene and pyrazine.

The property of interest here is a spectrum, either an absorption spectrum (pyrazine) or photo-electron spectrum (butatriene and allene). The spectrum  $\sigma(\omega)$  is calculated by Fermi's golden rule [8]:

$$\sigma(\omega) = a(\omega) \sum_n \left| \langle \Psi_n^f | \hat{T} | \Psi_0^i \rangle \right|^2 \delta(\omega + E_0^i - E_n^f). \quad (33)$$

Here, the final states  $\{|\Psi_n^f\rangle\}$  represent eigenstates of the Hamiltonian with energies  $E_n^f$ , and  $\hat{T}$  denotes the appropriate transition operator. The initial state  $|\Psi_0^i\rangle$  (with energy  $E_0^i$ ) is the electronic and vibrational ground state of the molecule. The pre-factor  $a(\omega)$  is proportional to  $\omega$  for absorption spectra but is taken constant for ionisation spectra.

The spectrum is conveniently evaluated by Fourier transform of the autocorrelation function. To this end one defines the initial state of the propagation by

$$\Psi(0) = \hat{T} |\Psi_0^i\rangle. \quad (34)$$

As we assume a vertical transition (Condon approximation),  $\Psi(0)$  is the ground-state wavepacket placed on an excited or ionic diabatic potential energy surface.

The autocorrelation function is defined as

$$C(t) = \langle \Psi(0) | \Psi(t) \rangle = \langle \Psi^*(t/2) | \Psi(t/2) \rangle, \quad (35)$$

where the second form is only valid for a real initial wavefunction and a symmetric Hamiltonian. These requirements are fulfilled here and the second form is particularly useful in conjunction with the MCTDH method as it reduces the required length of propagation by a factor of two.

The absorption (or ionisation) cross-section can now be expressed as

$$\sigma(\omega) = a(\omega) \pi^{-1} \text{Re} \int_0^\infty C(t) e^{i(\omega + E_0^i)t} dt. \quad (36)$$

To compensate for the finite time of the propagation, the autocorrelation must be multiplied by a function that ensures it goes to zero at the end of the propagation. If this is not done, spurious structures (known as Gibbs phenomenon) will be seen in the spectrum. We choose the function

$$g(t) = \cos\left(\frac{\pi t}{2T}\right) \theta\left(1 - \frac{|t|}{T}\right) \quad (37)$$

for this task, where  $T$  is the length of the propagation, and  $\theta$  is the Heaviside step function. In order to compare the calculated spectrum with the experimental one, it may also be necessary to multiply the autocorrelation function with a damping factor

$$f(t) = \exp(-t/\tau) \quad (38)$$

where  $\tau$  is a time constant describing a phenomenological broadening of the spectrum due to, e.g. spectral resolution. This is equivalent to convoluting the spectrum with a Lorentzian function of full width at half-maximum (FWHM) of  $\Gamma[\text{eV}] \approx 1.31/\tau[\text{fs}]$ .

## 4.2 The butatriene cation $\tilde{X}$ / $\tilde{A}$ manifold

The first demonstration [8] of the dramatic effects a conical intersection may have on the dynamics of a molecular system was given through the computation of the photo-electron spectrum of butatriene ( $\text{C}_4\text{H}_4$ ). The measured spectrum [30] of the ground ( $\tilde{X}$ ) and first excited ( $\tilde{A}$ ) electronic states of the cation of this planar molecule is shown in Fig. 1 (a). Two intense peaks are seen which lie at the energies expected for the two electronic states. Unexpectedly, between these peaks is also a structured region which is due to the strong vibronic coupling between these states. The calculation could reproduce the measured spectrum and in particular the so called ‘‘mystery band’’, i. e. the intensity between the two main peaks. As the ‘‘mystery band’’ is not understandable in an adiabatic picture, this early study vividly proved the importance of nonadiabatic effects caused by a conical intersection when computing spectra.

The molecule has  $D_{2h}$  symmetry and the states are  $\tilde{X}^2\text{B}_{2g}$  and  $\tilde{A}^2\text{B}_{3u}$ . Thus from the symmetry arguments of the vibronic coupling model the linear coupling is due to modes with  $A_u$  symmetry, of which butatriene has only one, the  $\nu_5$  torsional motion. Four modes of  $A_g$  symmetry are present and able to be tuning modes, but the  $\nu_{14}$  central C—C stretch dominates with a coupling constant an order of magnitude larger than the coupling constants of the other modes.

Using this information a two-dimensional vibronic coupling model Hamiltonian, Eq. (4), has been set up and parametrised using ab initio calculated data [8, 10]. Fig. 2 shows the adiabatic potential energy surfaces for these states in the space of the two dominant vibrational modes. These surfaces are the eigenvalues of the

diabatic potential matrix,  $\mathbf{W}$ , in Eq. (3). In Fig. 2 (a) the vibronic coupling has been set to zero. Two inter-penetrating wells are seen, representing the uncoupled oscillators, shifted along the symmetric vibrational coordinates. In Fig. 2 (b) the effect of including the inter-state coupling is obvious: the lower well has broadened and split into a double well. The upper and lower surfaces also now meet at a point, the conical intersection.

The spectrum from this two-dimensional model is shown in Fig. 1(b). The spectrum has been broadened by multiplying the autocorrelation function with Eq. (38) with a time constant of 35 fs. This is equivalent to convoluting the peaks in the spectrum with a fairly broad Lorentzian with 40 meV FWHM. The agreement with the experimental spectrum is very good: proof that the central band is due to a breakdown of the Born-Oppenheimer approximation by vibronic coupling.

To see the effect of the vibrational modes which have been neglected in this 2-mode model, an 18-mode model Hamiltonian has also been parametrised including all the vibrational modes, and coupling coefficients up to second order (quadratic and bilinear) [12]. The spectrum from this 18-mode model is shown in Fig. 1(c). Little change is seen, showing that in this case the two modes previously identified dominate the dynamics. This will be shown not to be the case in other systems.

Although the 2-mode model can reproduce the experiment astonishing well, it can do so only by using effective coupling constants. To reproduce the experiment, the coupling constants had to be manually adjusted and differ from the ab-initio values by factors between 1.3 and 1.5. In contrast, the 18-mode model used the unmodified ab initio values for all coupling constants except for the linear interstate coupling constant  $\lambda$ . The latter was increased by 19% with respect to the ab initio data. (See Ref. [12] for details). The rather large changes required for the parameters of the 2-mode model indicate that here the two modes act as effective modes, partially accounting for the neglected modes through their modified parameters.

As this system can be described by a 2-mode model, we are able to plot the complete nuclear wavefunction as it evolves in time, and this provides a base against which other systems can be compared. In Fig. 3 the time-evolution of the system density is shown in the diabatic picture. The initial wavepacket is the ground state vibrational eigenfunction, a Gaussian function centred around  $\mathbf{Q} = 0$ , projected into the upper state. Initial motion remains in this state, moving across the upper well until the conical intersection is reached. At this point, which is reached after only a few femto seconds, density is transferred to the lower state, appearing on two sides of the cone. The density on both surfaces then travels around the respective minima, and returns to the intersection after 40 fs, when interstate crossing (in both directions) occurs once more. In this undamped two-mode system, this pattern is repeated ad infinitum.

In Fig. 4 the time-evolution of a wavepacket is shown again, but this time in the adiabatic picture. As the conical intersection lies within the Condon region, the excitation results in a small occupation of the lower adiabatic state besides mainly occupying the upper. Following the evolution of the packet on the upper surface, the cone in Fig. 2(b), the density quickly disappears, and is transferred to the lower state within 30 fs. The dynamics on the lower surface is more complicated, but similar to that in the diabatic picture, with the density again flowing around the minimum, coming away from two sides of the intersection. After 40 fs the density returns to the intersection point and some re-crossing to the upper state is seen.

### 4.3 The allene cation $\tilde{A}$ / $\tilde{B}$ manifold

Despite its chemical similarity to butatriene, allene ( $C_3H_4$ ) has a very different set of electronic states due to the fact that the ground state equilibrium structure is  $D_{2d}$ , with the  $CH_2$  groups perpendicular to one another. The ground state of the

cation is doubly degenerate,  $\tilde{X}^2E$ , and forms an example of the relatively rare  $E \otimes \beta$  Jahn-Teller interaction [31,32]. An even more interesting system is found in the next band of the photoelectron spectrum, which is shown in Fig. 5(a). At low energies a set of ordered peaks are seen, with the structure being washed out at high energies. This band in fact contains two states, the close lying  $\tilde{A}^2E$  and  $\tilde{B}^2B_2$  states [33]. The  $\tilde{A}^2E$  is again a  $E \otimes \beta$  Jahn-Teller state, which then further interacts with the  $\tilde{B}^2B_2$  state via pseudo-Jahn-Teller coupling. This system provides a challenge for dynamics calculations, as all fifteen vibrational modes couple to first order.

Early calculations focused on the low energy  $\tilde{A}^2E$  band structure [32]. Here the four doubly degenerate vibrations can be ignored as they do not couple these states. Of the remaining seven modes, the most strongly coupled of each symmetry type was taken to provide a 3-mode model with the  $\nu_4$  ( $B_1$ ),  $\nu_7$  ( $B_2$ ), and  $\nu_2$  ( $A_1$ ) modes. The first two of these provide the Jahn-Teller active modes, coupling the degenerate electronic states. From inspection of the orbitals, the  $B_1$  torsional mode provides the off-diagonal coupling and  $B_2$  the on-diagonal coupling. The  $A_1$  mode is also activated by excitation from the neutral ground state, and appears on the diagonal of the Hamiltonian. The coupling constant is however the same for both states. After adjustment of the parameters, this model is able to adequately describe the experimental spectrum.

A later study [34] added the pseudo-Jahn-Teller coupling to the  $\tilde{B}^2B_2$  state to this model. This resulted in a 10-mode model, the spectrum of which is shown in Fig 5(b). The two parts of the spectrum are plotted separately to show that the peaks at either end can be assigned to each state, with the overlap in the middle forming a structureless band.

Including all 15 vibrational modes, however, was not possible within the linear model in a satisfactory manner. In particular, inclusion of the  $\nu_3$  ( $A_1$ ) mode provided problems as it is also significantly coupled to the excitation. The problem was traced to the lack of second-order coupling. On calculating these parameters, it was found that the  $\nu_2$  and  $\nu_3$  modes were strongly coupled, and undergo Duschinsky rotation. No correction of the first order terms was then required and the resulting spectrum from the 15-mode model is shown in Fig. 5(c) [35].

How this second order model changes the interpretation of the spectrum arising from the Jahn-Teller active  $\tilde{A}$  band is made clear in Fig. 6. In (a) the spectrum obtained from a 2-mode model with the adjusted parameters of Ref. [32] is shown. The progression of peaks is in good agreement with the experimental spectrum, and these can then be assigned to the  $\nu_7$  and  $\nu_2$  vibrations, and overtones of these. Fig. 6 (b) shows the same spectrum from the three most important modes from the second order model. The interpretation here is that the lower peak is due to a combination of  $\nu_2$  and  $\nu_3$  vibrations, while the higher peak is from  $\nu_7$ . This interpretation is more satisfactory as it fits the ab initio data better. Moreover, the inclusion of  $\nu_3$  and – to a lesser extent – of all the other neglected modes significantly increases the density of states leading to an enhanced spectral intensity in the vicinity of 15 eV (see Fig. 5).

In Fig. 7 the time evolution of the diabatic state populations in the  $\tilde{A}/\tilde{B}$  manifold are plotted. In (a) the results are shown after excitation takes place from the neutral ground state to the  $B_2$  state. The population is seen to rapidly decay, transferring to the lower energy  $E$  state within 20 fs. Weak recurrences are then seen with a time period of 50 fs.

In Fig. 7(b) the population is shown after excitation to one component of the  $E$  state. Population transfer takes place initially to the  $B_2$  state before being transferred on to the other  $E$  component. This process continues in an oscillatory fashion with a frequency of approximately 25 fs, which corresponds to the frequency of the  $\nu_2$  mode. This process is in fact a step wise electron transfer process [36]. The orbitals of the states are plotted in Fig. 7(a), and it can be seen that excitation

to a component of the E state corresponds to removing an electron from one end of the molecule. Population transfer corresponds to transferring electron density from the other end to fill this hole. The B<sub>2</sub> state, which has density all along the conjugated system, thus plays a role in this transfer.

#### 4.4 The pyrazine S<sub>1</sub> / S<sub>2</sub> manifold

A classic example of the effect of a conical intersection on the photophysics of a molecule is found in the adsorption spectrum of the pyrazine molecule [37, 38]. In contrast to the S<sub>1</sub> (B<sub>3u</sub>) band, which has a well defined vibronic structure, the S<sub>2</sub> (B<sub>2u</sub>) state gives rise to a very broad band with little structure. This is reproduced in Fig. 8(a).

Using the vibronic coupling model, a conical intersection has been identified and characterized [39]. In the linear model, there is one coupling mode,  $\nu_{10a}$  with B<sub>1g</sub> symmetry, and five possible tuning modes with A<sub>g</sub> symmetry. The spectrum from a linear 4-mode model, which ignores the two weakest coupled tuning modes, is shown in Fig. 8(b), and is seen to agree very well with the experimental one. To obtain this spectrum, however, a large phenomenological broadening has been added, with the spectrum being convoluted with a broad Lorentzian of 37 meV FWHM ( $\tau = 35$  fs in Eq. (38)).

In Fig. 8(c) the spectrum is shown from a second order model, which includes all 24 modes [11]. Here a damping function with a time-constant of only 150 fs is required for good agreement with the experimental spectrum, equivalent to the broadening due to the spectrometer. Thus, while the major features of the spectrum can be accounted for by the 4-mode model, its envelope can only be explained by including all the modes.

This calculation was a formidable task. Alone setting up the Hamiltonian, which involved calculating and testing 102 coupling constants, was very time consuming. 24 vibrational modes and 2 coupled electronic states is well beyond the reach of standard wavepacket methods. This was possible only by using the MCTDH method, with the refinements of combined modes, and the multi-set formulation. Even so, 2,771,440 configurations were required for good quality results and the propagation of 150 fs required 650 MB and 485 hours on a Cray T90 vector computer. In contrast, the 4-mode model required 20 minutes and 16 MB on an IBM RS/6000 power 2 workstation.

#### 4.5 The pyrazine molecule viewed as a system coupled to a bath

One question that arises in the pyrazine study is as to whether it is really necessary to accurately describe the 20 weakly-coupled modes, or could a weakly coupled bath lead to the same result, namely a seemingly homogeneous broadening of the 4-mode model spectrum. A model in which the 4-mode linear model coupled to a weak bath has thus also been set up [40]. The bath modes are coupled linearly to each state, and provide pathways for the dephasing of the wavepacket. We have studied this model using the MCTDH method [14], with which it was possible to perform accurate quantum dynamical calculations including up to 20 bath modes.

These calculations demonstrate the scaling of the MCTDH method with system size. The computer resources required are summarized in Table 1. For comparison it is indicated how many MCTDH particles (effective degrees of freedom in the calculation) were used, and how many configurations were required. Both memory requirements and CPU-time required increase rapidly: not exponentially, however, but roughly as dimension to the third power. For a 120 fs propagation, this 4-mode

model, which is slightly different from that used above, required 4MB and 6 minutes, while the system coupled to 20 bath modes required 687MB and 3100 minutes ( $\approx 52$ h). Even so, the 24-mode calculations are easy to make on a normal workstation. The much longer time required for the 24-mode second-order pyrazine model calculations shown above is due to the large number of terms in the Hamiltonian required.

The spectra from the 4-mode model coupled to 0, 5, 10, and 20 bath modes are plotted in Fig. 9(a)-(d), and the addition of the bath clearly results in the structure of the spectrum being washed out. The experimental spectrum is, however, not obtained. The effect of the bath modes is made clear in Fig. 10(a)-(d), in which the absolute values of the autocorrelation function for the 4-mode system with 0, 5, 10, and 20 bath modes is plotted. Just the strongest 5 bath modes lead to a significant damping of the oscillations in the function. This is simply due to the extra volume of phase-space available in which the wavepacket dissipates, and thus dephases. It is clear from this plot that the bath model chosen does not lead to a homogenous broadening of the spectrum, as extra structure is also added (see for example the first peak). Interestingly, even with the 20-mode bath a definite beat-like structure is present, and it is as if the bath is filtering the spectrum - while the wavepacket at most frequencies is dephased, certain frequencies survive [28].

Fig. 11 shows the time-evolution of the population of (a) diabatic and (b) adiabatic  $S_2$  states. In all cases, the population decays sharply over the first 40 fs. After approximately 80 fs a recurrence occurs, and population is transferred back from the  $S_1$  to the  $S_2$  state. The adiabatic populations exhibit a faster, and more complete, population transfer. The recurrence is also much smaller. In both diabatic and adiabatic pictures, the presence of the bath increases the rate and amount of transfer. With 10 bath modes, the population of the adiabatic  $S_2$  state goes very nearly to zero over this time-scale. The 20 bath mode model adiabatic state populations could not be calculated due to the technical problem of the diabatic - adiabatic transformation for a system of this size.

We finally mention that the system/bath picture for studying the pyrazine spectrum has been adopted by two other publications [41,42]. There, however, the bath was treated implicitly by dissipative operators of the Lindblad type.

## 5 Conclusions

A very useful starting point for the study of nonadiabatic processes, which are common in photochemistry and photophysics, is the vibronic coupling model Hamiltonian. The model is based on a Taylor expansion of the potential surfaces in a diabatic electronic basis, and it is able to correctly describe the dominant feature resulting from vibronic coupling in polyatomic molecules: a conical intersection. The importance of such intersections is that they provide efficient non-radiative pathways for electronic transitions. Not only is the position and shape of the intersection described by the model, but it also predicts which nuclear modes of motion are coupled to the electronic transition which takes place as the system evolves through the intersection.

The modes involved to first order, i.e. including coupling terms linear in the nuclear coordinates, are coordinates of the correct symmetry required to couple the electronic states, as well as the totally symmetric coordinates, which modulate the energy gap. These are often only a few modes in total, and may provide a reasonable description of the major physics of the system. Neglecting further the most weakly coupled modes, this can result in small, 2, 3 or 4 mode models, which can then be treated using standard wavepacket methods to obtain a full quantum mechanical solution of the problem.

To second order, however, all degrees of freedom are involved. Even for small molecules (5–12 atoms, say) these systems are no longer accessible to standard quantum dynamics methods. Here, the MCTDH method becomes an essential tool. MCTDH is an efficient wavepacket propagation method, accurate, yet flexible, and applicable to a wide range of problems. Its ability to include more degrees of freedom than conventional wavepacket methods is of particular importance in the study of the multi-dimensional dynamics associated with non-adiabatic processes. Using this method we have been able to treat a number of typical non-adiabatic systems completely up to second order, i.e. including all degrees of freedom.

Our calculations show that these second order terms are important for a quantitative description of non-adiabatic systems. This is demonstrated in the pyrazine  $S_1/S_2$  system, where a reduced 4-mode model provides a qualitative picture with the main peaks of the spectrum in the correct places. The addition of second order terms and all degrees of freedom, results in the correct spectral envelope also being produced by the model. Also in the allene  $\tilde{A}/\tilde{B}$  system, the second order terms are required, not only for the correct description of the Duschinsky rotation in the excited state, but also for the high spectral density between the two bands. Even in the butatriene  $\tilde{X}/\tilde{A}$  system, in which second order terms play a minor role in the description of the spectral band, the inclusion of these terms means that the ab initio data could be taken with minimal adjustment, whereas a reduced dimensionality model required significant adjustment of the expansion parameters.

Using the MCTDH method we have thus been able to provide full-dimensionality calculations on the quantum dynamics of a molecular system passing through a conical intersection. These calculations not only give insight into the factors required for the description of such systems, but also provide benchmarks for comparison with results from more approximate methods.

Let us summarize the major points:

- The vibronic coupling Hamiltonian provides a realistic model for accurately describing the short-time multi-mode dynamics in non-adiabatic systems.
- The computations have shown that a multi-mode treatment is essential for correctly describing the dynamics in the presence of a conical intersection.
- The advent of MCTDH has made it possible to solve the (second-order) vibronic coupling Hamiltonian of small to medium sized molecules (5 – 12 atoms, say), including *all* internal degrees of freedom. In fact, it is the combination of the vibronic coupling model with MCTDH which is numerically so successful. The vibronic coupling model provides a realistic multi-mode Hamiltonian, and this Hamiltonian is, from its *ansatz*, in the product form advantageous for MCTDH. MCTDH then solves the dynamics problem accurately and efficiently.

## References

- [1] *Time-dependent methods for quantum dynamics*, edited by K. C. Kulander (Elsevier, Amsterdam, 1991).
- [2] *Numerical Grid Methods and their Application to Schrödinger's Equation*, edited by C. Cerjan (Kluwer Academic Publishers, Dordrecht, 1993).
- [3] R. Kosloff, *Ann. Rev. Phys. Chem.* **45**, 145 (1994).
- [4] H.-D. Meyer, U. Manthe, and L. S. Cederbaum, *Chem. Phys. Lett.* **165**, 73 (1990).
- [5] U. Manthe, H.-D. Meyer, and L. S. Cederbaum, *J. Chem. Phys.* **97**, 3199 (1992).
- [6] M. H. Beck, A. Jäckle, G. A. Worth, and H.-D. Meyer, *Phys. Rep.* **324**, 1 (2000).
- [7] F. Duschinsky, *Acta Physicochim. URSS* **7**, 551 (1937).
- [8] L. S. Cederbaum, W. Domcke, H. Köppel, and W. von Niessen, *Chem. Phys.* **26**, 169 (1977).
- [9] L. S. Cederbaum and W. Domcke, *Adv. Chem. Phys.* **36**, 205 (1977).
- [10] H. Köppel, W. Domcke, and L. S. Cederbaum, *Adv. Chem. Phys.* **57**, 59 (1984).
- [11] A. Raab, G. Worth, H.-D. Meyer, and L. S. Cederbaum, *J. Chem. Phys.* **110**, 936 (1999).
- [12] C. Cattarius, G. A. Worth, H.-D. Meyer, and L. S. Cederbaum, *J. Chem. Phys.* **115**, 2088 (2001).
- [13] H.-D. Meyer, in *The Encyclopedia of Computational Chemistry*, edited by P. v. R. Schleyer *et al.* (John Wiley and Sons, Chichester, 1998), Vol. 5, pp. 3011–3018.
- [14] G. A. Worth, H.-D. Meyer, and L. S. Cederbaum, *J. Chem. Phys.* **109**, 3518 (1998).
- [15] J. C. Light, I. P. Hamilton, and J. V. Lill, *J. Chem. Phys.* **82**, 1400 (1985).
- [16] J. C. Light, in *Time-Dependent Quantum Molecular Dynamics*, edited by J. Broeckhove and L. Lathouwers (Plenum, New York, 1992), pp. 185–199.
- [17] P. A. M. Dirac, *Proc. Cambridge Philos. Soc.* **26**, 376 (1930).
- [18] J. Frenkel, *Wave Mechanics* (Clarendon Press, Oxford, 1934).
- [19] A. Jäckle and H.-D. Meyer, *J. Chem. Phys.* **109**, 3772 (1998).
- [20] U. Manthe, *J. Chem. Phys.* **105**, 6989 (1996).
- [21] M. H. Beck and H.-D. Meyer, *Z. Phys. D* **42**, 113 (1997).
- [22] U. Manthe and A. D. Hammerich, *Chem. Phys. Lett.* **211**, 7 (1993).
- [23] A. D. Hammerich *et al.*, *J. Chem. Phys.* **101**, 5623 (1994).
- [24] J.-Y. Fang and H. Guo, *J. Chem. Phys.* **101**, 5831 (1994).

- [25] G. A. Worth, H.-D. Meyer, and L. S. Cederbaum, *J. Chem. Phys.* **105**, 4412 (1996).
- [26] H. Wang, *J. Chem. Phys.* **113**, 9948 (2000).
- [27] M. Ehara, H.-D. Meyer, and L. S. Cederbaum, *J. Chem. Phys.* **105**, 8865 (1996).
- [28] G. A. Worth, H.-D. Meyer, and L. S. Cederbaum, *Chem. Phys. Lett.* **299**, 451 (1999).
- [29] G. A. Worth, M. H. Beck, A. Jäckle, and H.-D. Meyer, The MCTDH Package, Version 8.2, (2000). See <http://www.pci.uni-heidelberg.de/tc/usr/mctdh/>.
- [30] F. Brogli *et al.*, *Chem. Phys.* **4**, 107 (1974).
- [31] L. S. Cederbaum, W. Domcke, and H. Köppel, *Chem. Phys.* **33**, 319 (1978).
- [32] C. Woywood and W. Domcke, *Chem. Phys.* **162**, 349 (1992).
- [33] P. Baltzer *et al.*, *Chem. Phys.* **196**, 551 (1995).
- [34] S. Mahapatra, L. S. Cederbaum, and H. Köppel, *J. Chem. Phys.* **111**, 10452 (1999).
- [35] S. Mahapatra *et al.*, *J. Phys. Chem. A* **105**, 5567 (2001).
- [36] G. Worth and L. Cederbaum, *Chem. Phys. Lett.* **348**, 477 (2001).
- [37] I. Yamazaki, T. Muraio, T. Yamanaka, and K. Yoshihara, *Faraday Discuss. Chem. Soc.* **75**, 395 (1983).
- [38] K. K. Innes, I. G. Ross, and W. R. Moonaw, *J. Mol. Spec.* **132**, 492 (1988).
- [39] C. Woywod, W. Domcke, A. L. Sobolewski, and H.-J. Werner, *J. Chem. Phys.* **100**, 1400 (1994).
- [40] S. Krempel, M. Winterstetter, H. Plöhn, and W. Domcke, *J. Chem. Phys.* **100**, 926 (1994).
- [41] T. Gerdts and U. Manthe, *J. Chem. Phys.* **106**, 3017 (1997).
- [42] A. Raab and H.-D. Meyer, *J. Chem. Phys.* **112**, 10718 (2000).

## Table and Figure captions

Table 1: Summary of computer resources required for calculations made using the MCTDH method on a 4-mode model of the  $S_1$  and  $S_2$  states of the pyrazine molecule after excitation to the  $S_2$  state, and coupled to harmonic oscillator baths of varying size [14]. The degrees of freedom (no. of bath modes + 4) were combined together into the no. of particles listed, and the no. of configurations required for converged calculations are given. The wavepacket was propagated for 120 fs.

bath modes	MCTDH particles	configurations	Memory (MB)	CPU time <sup>a</sup> (minutes)
0	4	10,575	3.7	6.3
5	4	74,024	48.9	185.0
10	5	142,350	52.5	196.9
20	7	3,759,552	686.5	3095.6

<sup>a</sup>on an IBM RS/6000 power2 workstation.

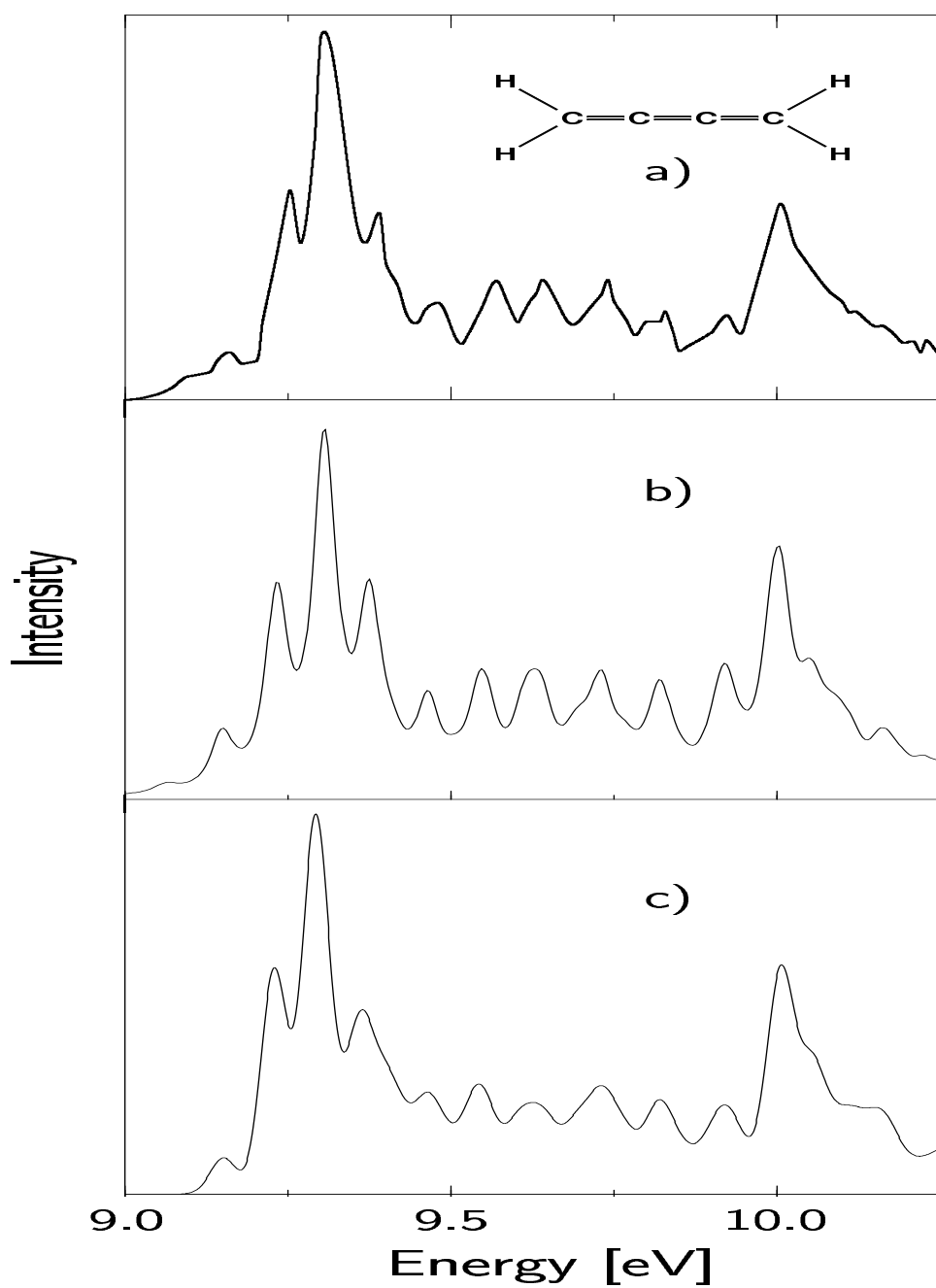


Figure 1: The  $\tilde{X}/\tilde{A}$  spectrum of the butatriene radical cation. (a) Experimental results from Ref. [30]. (b) 2-mode model from Ref. [10]. (c) 18-mode model from Ref. [12]. The model spectra are the Fourier Transform of the autocorrelation function calculated using the MCTDH wavepacket propagation method. A damping function of  $\tau = 55$  fs has been used.

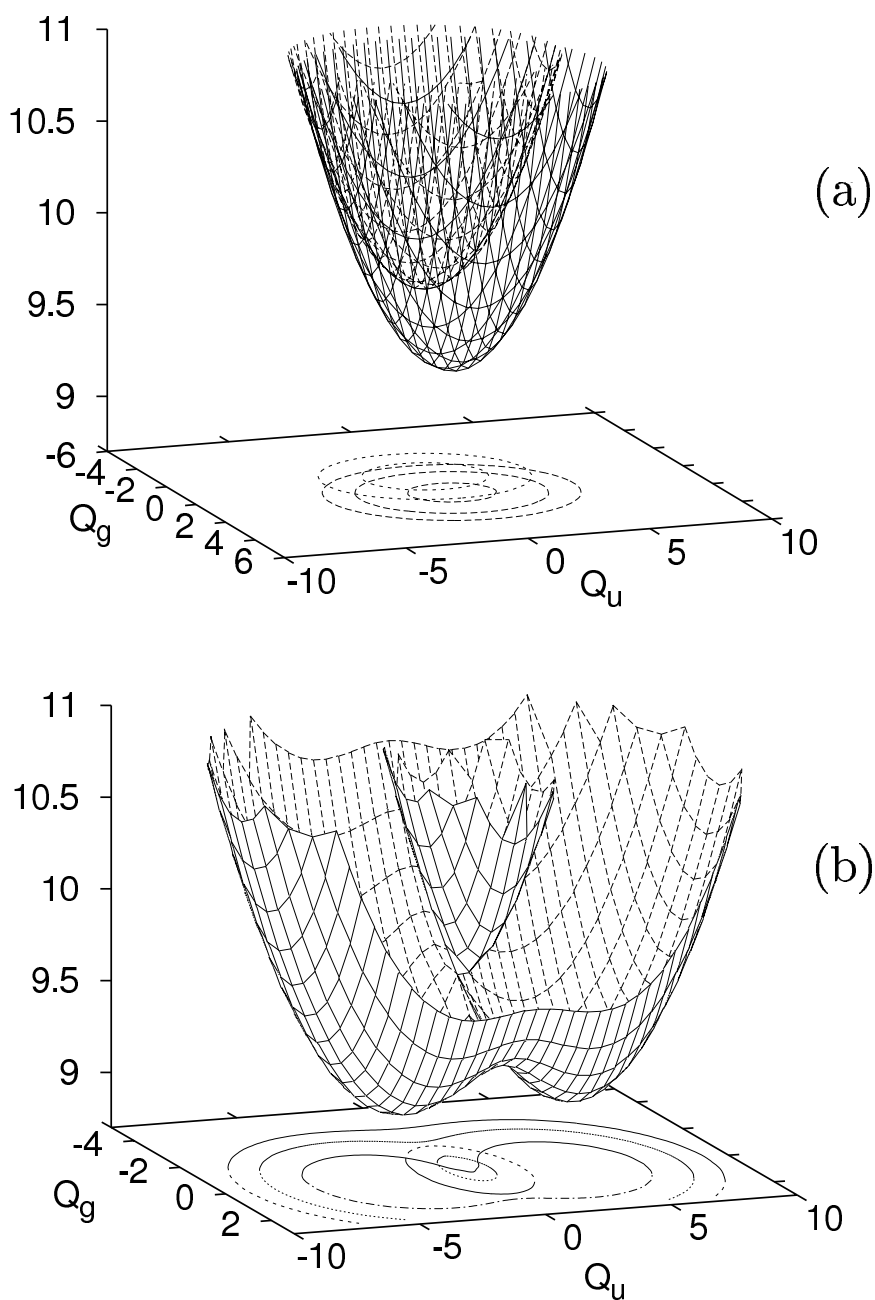


Figure 2: The potential energy surfaces for the  $\tilde{X}/\tilde{A}$  states of the butatriene radical cation. (a) in the absence of vibronic coupling. (b) including vibronic coupling.  $Q_u$  is the unsymmetric normal mode corresponding to the  $\nu_5(a_u)$  torsional mode, and  $Q_g$  is the symmetric normal mode corresponding to the  $\nu_{14}$  central C—C stretching vibration.

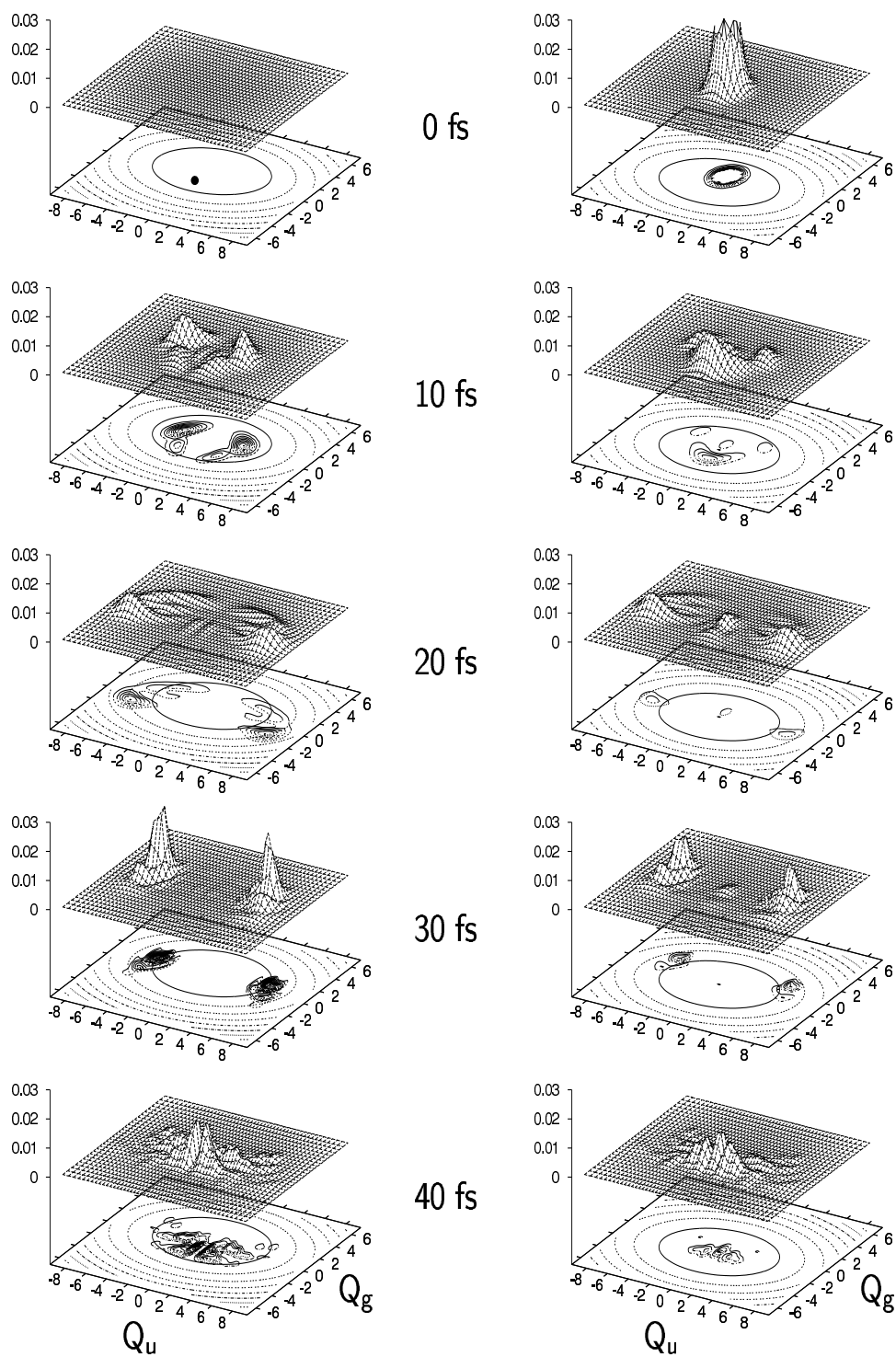


Figure 3: The time evolution of a wavepacket through the conical intersection between the  $\tilde{X}/\tilde{A}$  PES of the butatriene radical cation in the diabatic picture. The location of the conical intersection is indicated by a thick point in the uppermost plot. Left: first surface, right: second surface

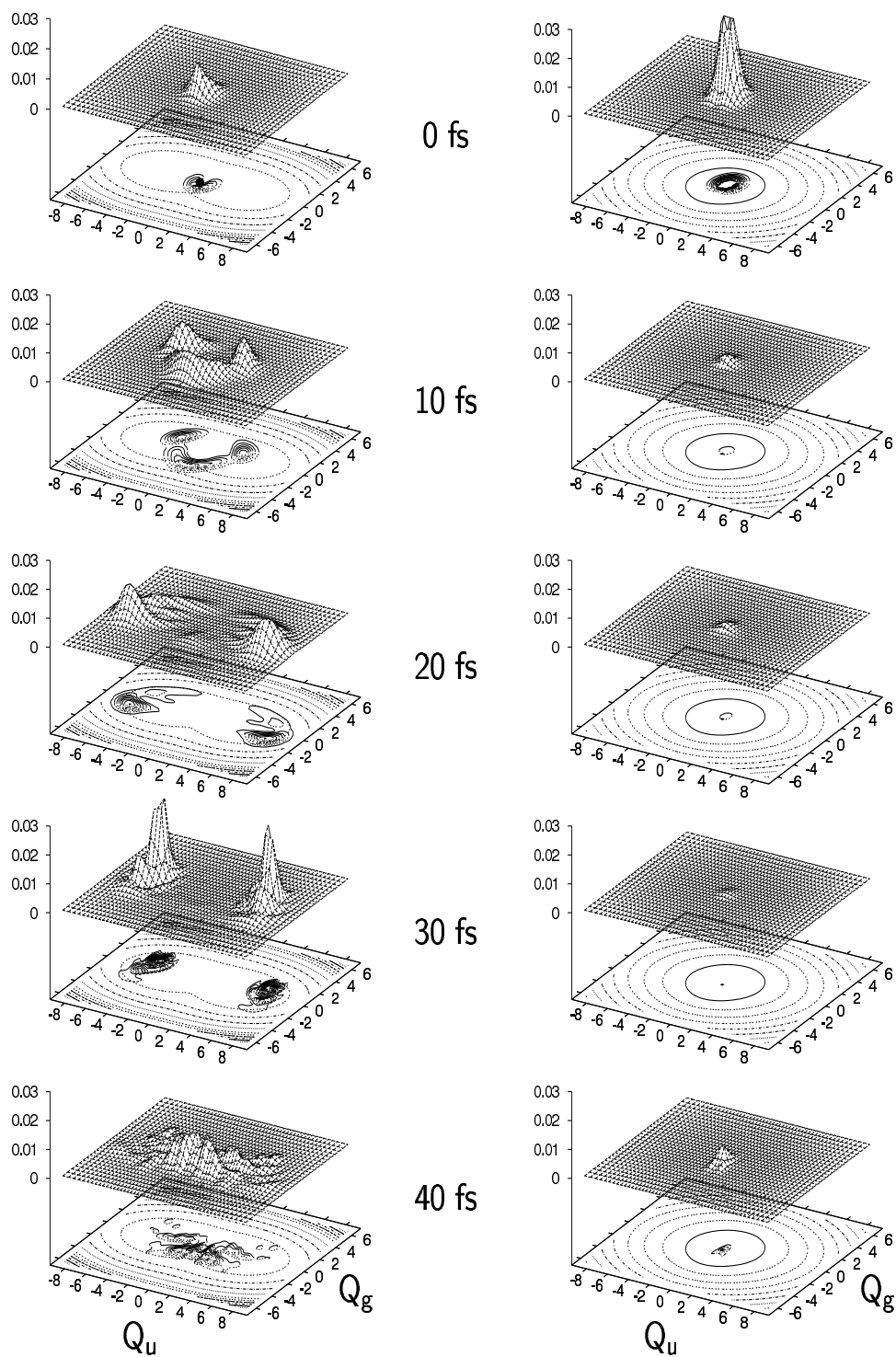


Figure 4: The time evolution of a wavepacket through the conical intersection between the  $\tilde{X}/\tilde{A}$  PES of the butatriene radical cation in the adiabatic picture. The location of the conical intersection is indicated by a thick point in the uppermost plot. Left: lower surface, right: upper surface

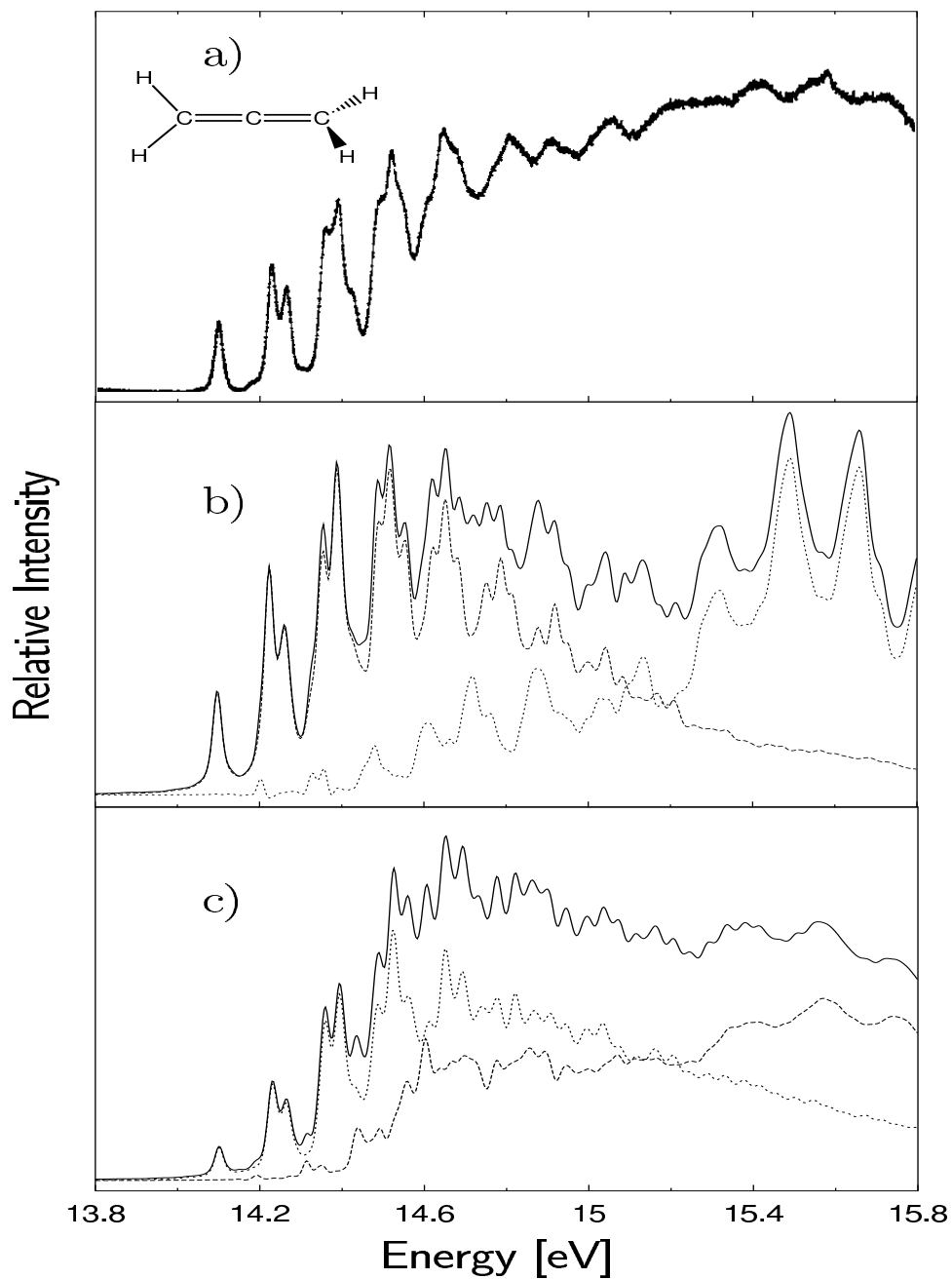


Figure 5: The  $\tilde{A}/\tilde{B}$  spectrum of the allene radical cation. (a) Experimental results from Ref. [33]. (b) 10-mode model from Ref. [34]. (c) 15-mode model from Ref. [35]. The model spectra are the Fourier Transform of the autocorrelation function calculated using the MCTDH wavepacket propagation method. A damping function of  $\tau = 50$  fs has been used.

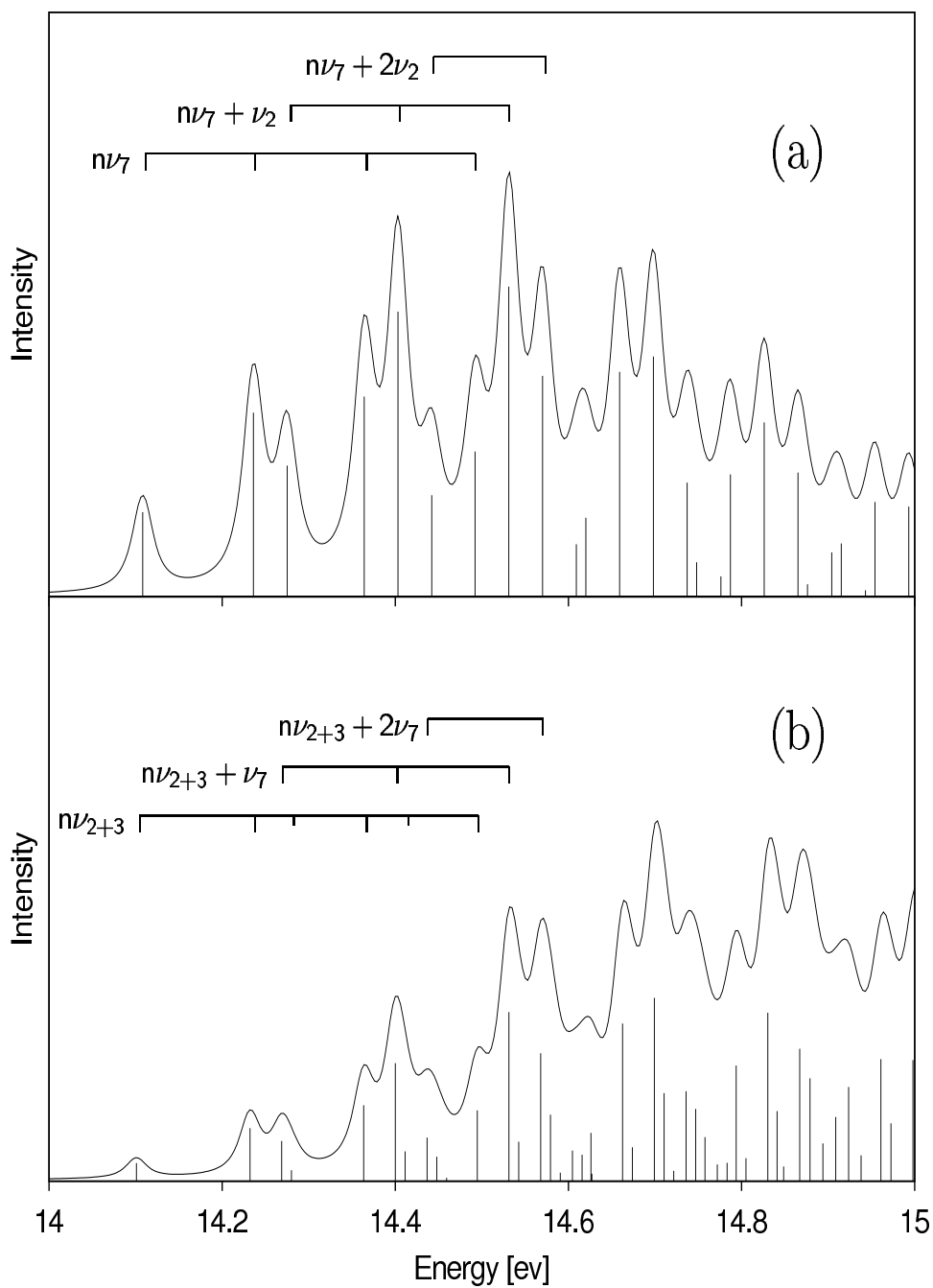


Figure 6: The spectrum of the Jahn-Teller split  $\tilde{A}E$  state of the allene radical cation using different reduced dimensionality models. (a) A linear 2-mode model including the vibrational modes  $\nu_2$  and  $\nu_7$  with parameters adjusted to fit the spectrum. (b) A 2nd order 3-mode model including the vibrational modes  $\nu_2, \nu_3$  and  $\nu_7$ .

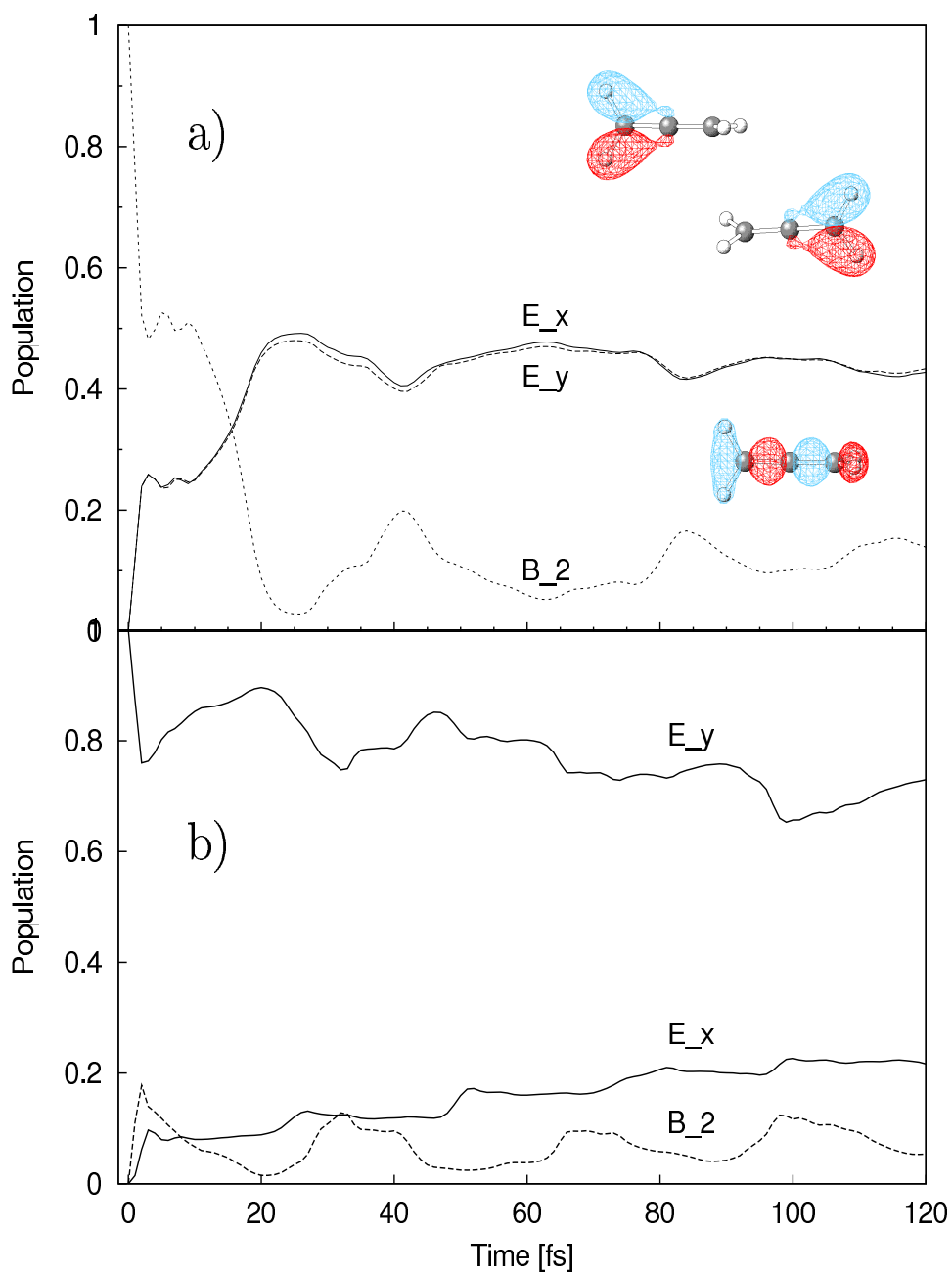


Figure 7: The time evolution of state population transfer in the  $\tilde{A}/\tilde{B}$  manifold of the allene radical cation after excitation to (a) the  $\tilde{B}(B_2)$  and (b) the  $\tilde{X}(E_y)$  diabatic state.

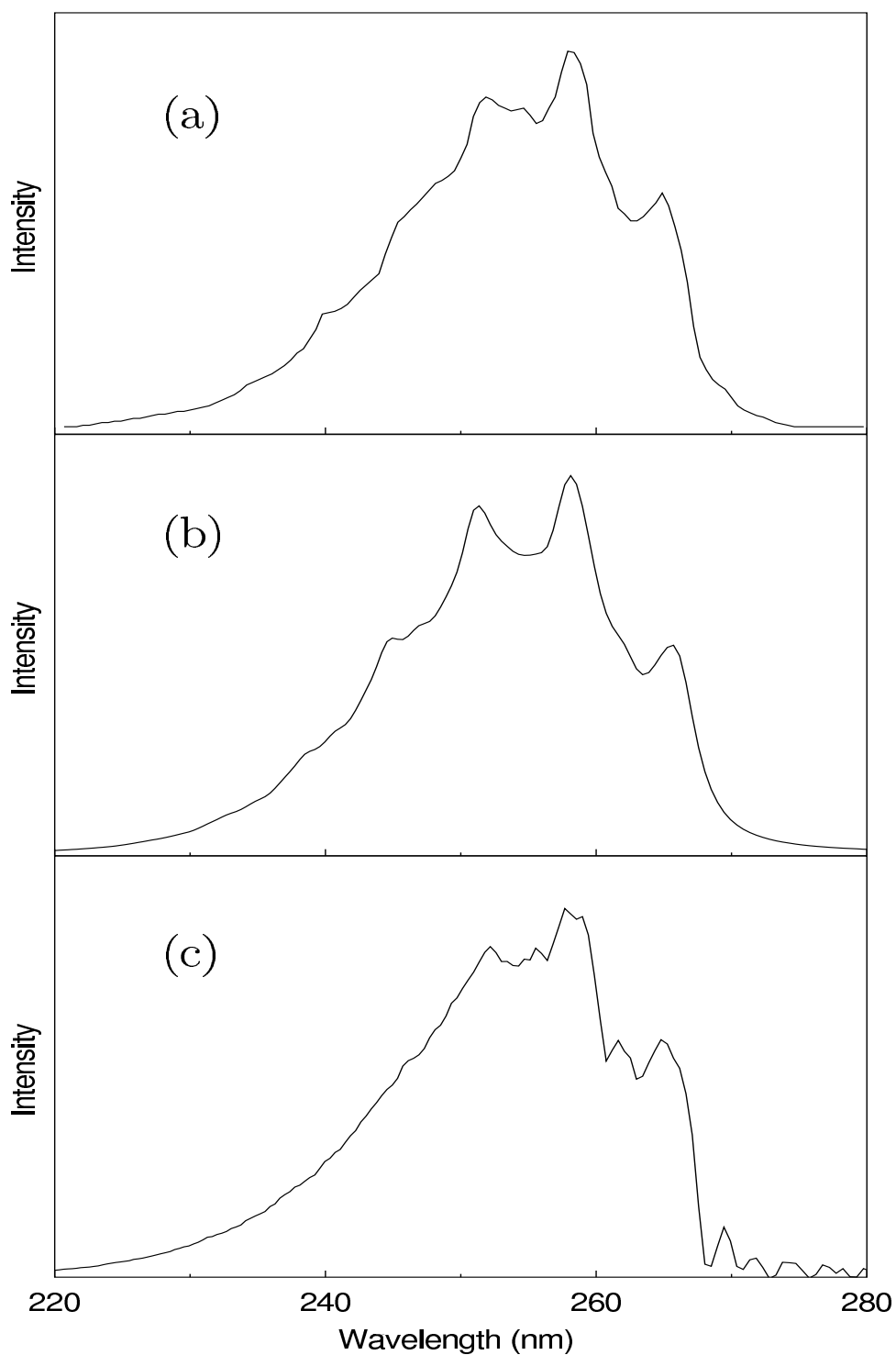


Figure 8: The  $S_2$  absorption spectrum of the pyrazine molecule (a). Experimental results from Ref. [37]. (b) 4-mode model from Ref. [39]. (c) 24-mode model from Ref. [11]. The model spectra are the Fourier Transform of the autocorrelation function calculated using the MCTDH wavepacket propagation method. A damping function of  $\tau = 30$  fs has been used in (b) and  $\tau = 150$  fs in (c).

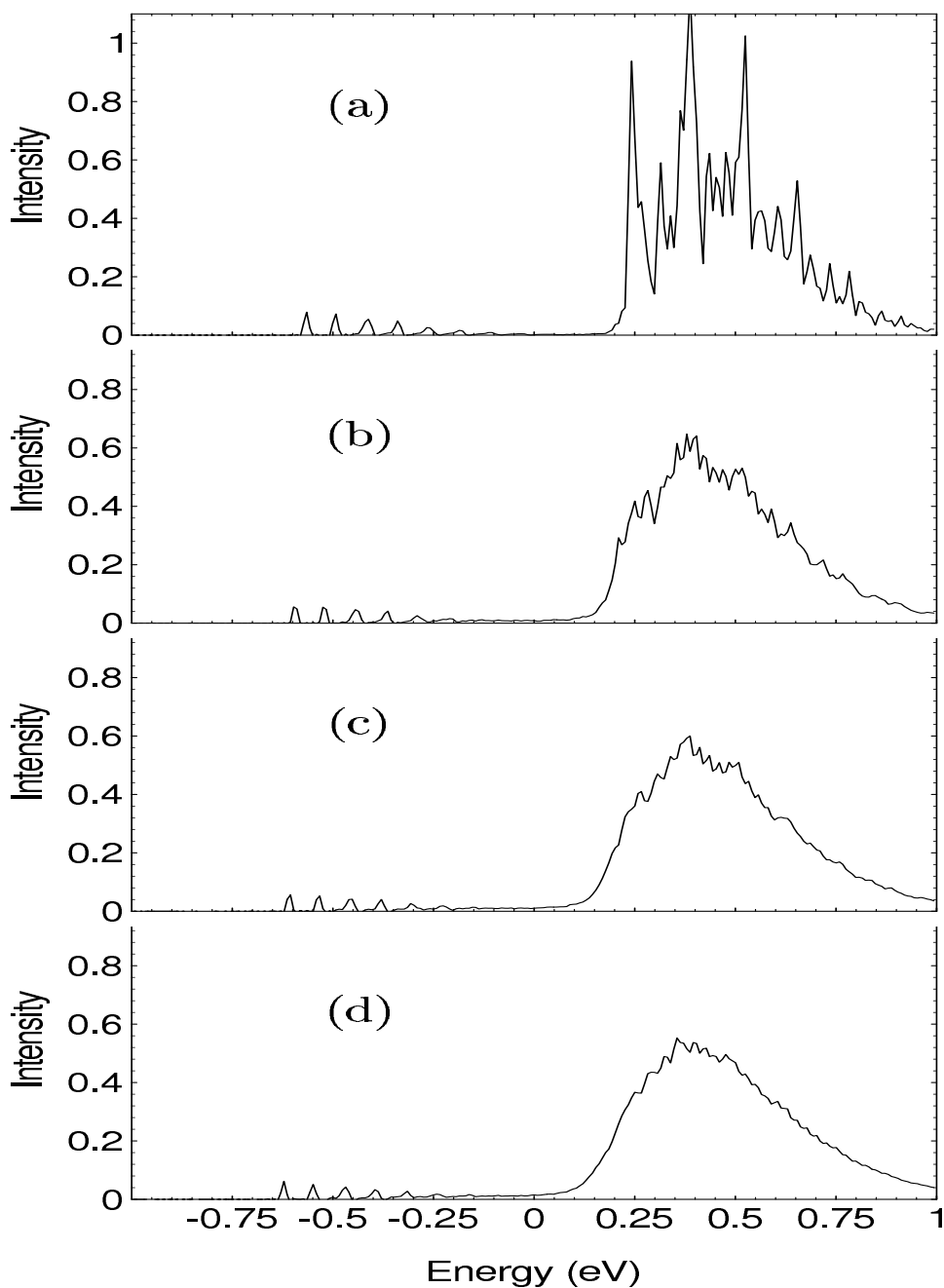


Figure 9: The effect of a bath on the spectrum of the 4-mode model for the  $S_1/S_2$  manifold of the pyrazine molecule after initial excitation to the  $S_2$  state. Taken from Ref. [14]. (a) No bath present. (b) 5 bath modes. (c) 10 bath modes. (d) 20 bath modes. The spectra are calculated from the Fourier Transform of the autocorrelation function. No phenomenological broadening has been added, but a cutoff function is used to remove artefacts due to the finite time-length (240 fs) of the autocorrelation function

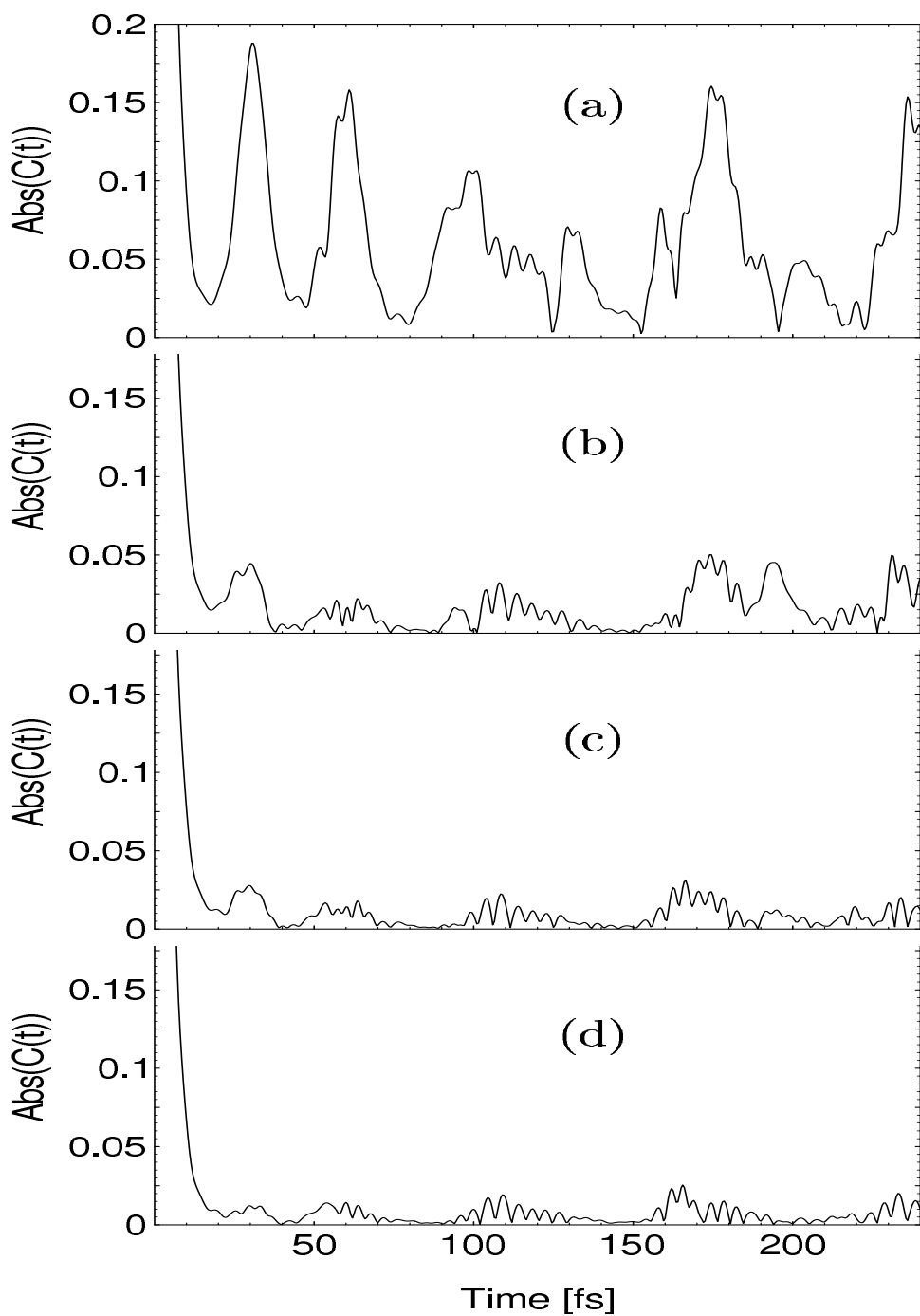


Figure 10: The effect of a bath on the autocorrelation function of the 4-mode model for the  $S_1/S_2$  manifold of the pyrazine molecule after initial excitation to the  $S_2$  state. Taken from Ref. [14]. (a) No bath present. (b) 5 bath modes. (c) 10 bath modes. (d) 20 bath modes.

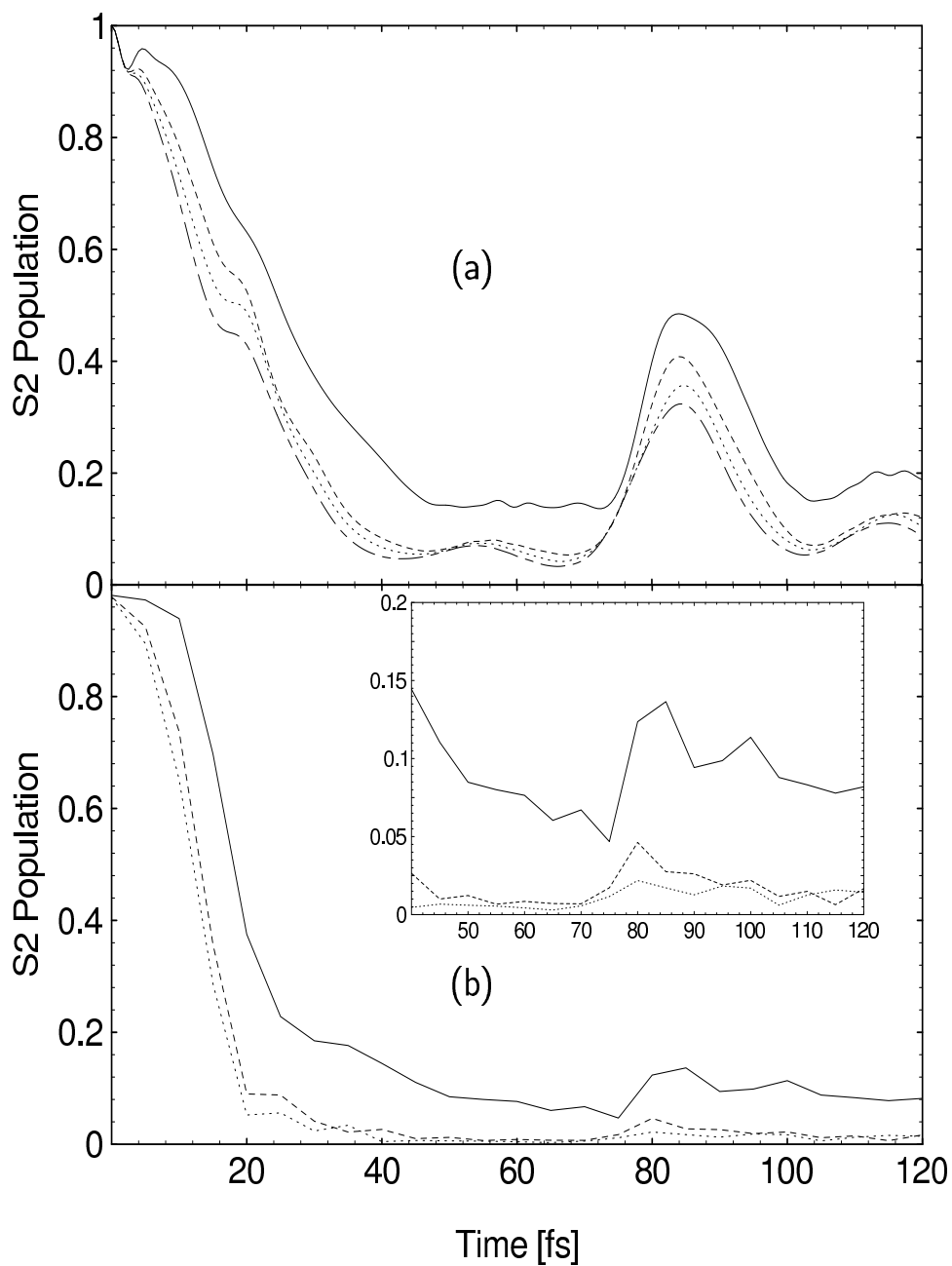


Figure 11: The effect of a bath on the rate of inter-state crossing in the 4-mode model of the pyrazine  $S_1/S_2$  manifold of the pyrazine molecule after initial excitation to the  $S_2$  state. Taken from Ref. [14]. (a) diabatic state population. (b) adiabatic state population. Full line: 0 bath oscillators. Dashed line: 5 bath oscillators. Dotted line: 10 bath oscillators. Dash-dot line 20 bath oscillators (diabatic state only).